*Progress In Electromagnetics Research, Vol. 114, 211–234, 2011*

# INSULATION FAULT DIAGNOSIS IN HIGH VOLTAGE POWER TRANSFORMERS BY MEANS OF LEAKAGE FLUX ANALYSIS

**M. F. Cabanas, F. Pedrayes, M. G. Melero, C. H. Rojas G. A. Orcajo, J. M. Cano, and J. G. Norniella**

Electrical Engineering Department, University of Oviedo
Edificio Departamental N° 4, Campus de Viesques s/n
33204 Gijón, Spain

**Abstract**—Power transformers in service are subjected to a wide variety of electrical, mechanical and thermal stresses capable of producing insulation faults. This type of failure figures amongst the most costly faults in distribution networks since it produces both machine outage and electrical supply interruption. Major research effort has therefore focused on the early detection of faults in the insulating systems of large high voltage power transformers. Although several industrial methods exist for the on-line and off-line monitoring of power transformers, all of them are expensive and complex, and require the use of specific electronic instrumentation. For these reasons, this paper will present the On-Line analysis of transformer leakage flux as an efficient alternative for assessing machine integrity and detecting the presence of insulating failures during their earliest stages. An industrial 400 kVA–20 kV/400 V transformer will be used for the experimental study. Very cheap, simple sensors, based on air core coils, will be used to measure the leakage flux of the transformer, and non-destructive tests will also be applied to the machine in order to analyse pre- and post-failure voltages induced in the coils.

## 1. INTRODUCTION

Compensation of leakage flux has been studied by several authors to avoid its undesirable effects [1–4], but leakage flux has also been proved as an useful tool for fault detection in a broad range of industrial

*Received 3 January 2011, Accepted 9 February 2011, Scheduled 1 March 2011*
Corresponding author: Manes Fernandez Cabanas (manes@uniovi.es).

devices. The use of different kind of probes and as well as different diagnosis techniques has been widely reported i.e., fault detection in metallic pipes and structural frames by means of non-destructive tests [5–7], fault detection in electric circuits [8–11] and fault detection in rotating machines [12–16]. Its application to the early detection of insulation faults in high voltage power transformers will be presented in this paper as a cheaper, efficient and simpler alternative to the use of conventional diagnosis methods.

Although different techniques exist for fault diagnosis in power transformers all of them present considerable limitations. Dissolved gas in oil analysis (DGA) [17–20], is a widely used method for the detection of hot spots inside the machine, but On-Line machine diagnosis with this procedure requires complex, expensive equipment capable of detecting the different gases dissolved in the transformer oil as a consequence of the failure. Partial discharge analysis [21, 22] has traditionally been used for quality control during the manufacturing process. The recent development of equipment that incorporates digital processing techniques, as well as the existence of new sensors, has led to its on-site application. However, sensor installation and interpretation of the results are both complex and expensive.

Power factor tests have also been applied to industrial transformers for several decades [23], yet this technique only gives a general indication of the status of a machine's insulation system and does not permit the detection of minor or marginal failures. Other new techniques such as RVM (Return Voltage Method), TDDS (Time Domain Spectroscopy, FTIF (Fourier Transform Infrared), NIR (Near-Infrared Spectroscopy), Power Factor as function of frequency, etc. are still being explored with very promising results. Nevertheless, industrial application remains expensive and complex, especially for generalised use in distribution transformers [24–26]. It is clear, then, that there is a need for simple, low cost methods for monitoring the condition of power transformers.

Leakage flux measurement is a cheap, simple and efficient alternative since it can be easily done in any kind of transformer. In the next sections the theoretical foundations of leakage flux analysis in three-phase transformers will be presented. Finite elements models of transformers with different type of windings, operating at normal and faulty conditions, will be used to demonstrate the ability of leakage flux to detect inter-turn insulation faults. The On-Line diagnosis method based on leakage flux analysis will be applied to a large 400 kVA high voltage transformer thus demonstrating the simplicity and reliability of this new diagnosis procedure.

## 2. THE LEAKAGE FLUX IN THREE-PHASE TRANSFORMERS

In power transformers, not all the flux produced by the primary winding passes through the secondary winding, nor vice versa. Instead, some of the flux lines exit the iron via the air. The portion of magnetic flux that goes through one of the transformer windings but not the other is called *leakage flux* [27], and the amount of leakage flux mainly depends on the ratio between the reluctance of the magnetic circuit and the reluctance of the leakage path [28]. Leakage flux lines in transformers are curved at the ends of the coils and flow through the air almost parallel to the winding axis [29]. The degree of curvature of the lines is affected by the distance between the coils and the machine's shield and the latter's distribution in the air is influenced by the type of winding used in the machine's construction [29]. Leakage flux lines in a healthy transformer have a horizontal axis of symmetry that passes through the middle of the magnetic core of the machine. When a short-circuit, or even a strong deformation, of one or several turns occurs, this symmetry is lost, therefore leakage flux can be used for the early diagnosis of insulation faults. Below, a simple theoretical approach for the analysis of the leakage flux in the windings of a power transformer is presented. This approximate analysis will show the symmetrical nature of leakage flux and will allow the establishment of the foundations for a diagnosis procedure. Theoretical results will be complemented with finite element models of transformers with different type of windings where the actual distribution of leakage flux will also be analysed.

The magnetic core and windings of a three-phase power transformer can be represented in an approximate way for the analysis of the leakage flux by means of the theory of the images [30, 32]. Electromagnetic problems involving a planar perfect electric or perfect magnetic conductor can be handled through the image principle, in which the surface is replaced by image sources that are mirror images of the sources of magnetic or electric potential [30]. This method can be easily applied to a core limb of a three-phase transformer in order to demonstrate the spatial symmetry of leakage flux. Figure 1 shows a graph with the application of this principle.

In the graph a core limb of a transformer with a single layer of winding is represented. For the sake of simplicity only the right side of the winding is used in the analysis. This simplification is reasonable since the contribution of the left-side winding to the leakage flux can be neglected if only the symmetrical or asymmetrical nature of the flux is being studied.

Taking into account that the normal component of the magnetic

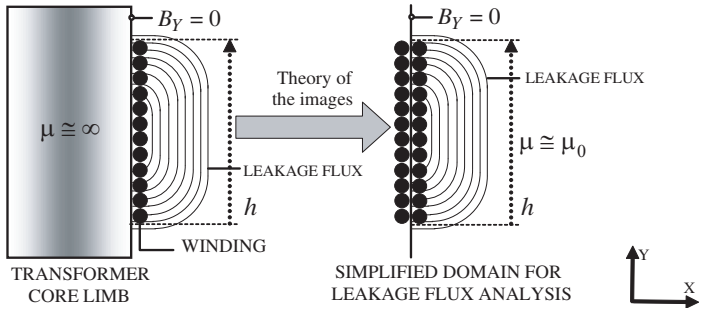


**Figure 1.** Application of the image principal to a core limb of a three-phase transformer.

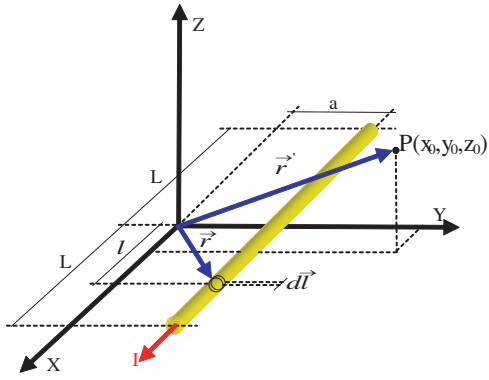


**Figure 2.** Single conductor and coordinates system.

induction $B_y$ is nil in the outside surface of the magnetic core, the theory of the images can be applied to the surface of the core limb. By simply adding a second layer of winding (image of the actual winding) at the internal face of the core, the same boundary conditions for the magnetic flux density are achieved. In this way, the leakage flux density in the outside of the core limb can be approximately calculated by obtaining the flux created by the two layers of conductors of the new simplified domain [31, 32].

The calculation of the flux created by the new domain can be easily done by integrating the flux density created by a single conductor [33]. Therefore, the first stage of the analysis will consists of the calculation of the normal component $B_y$ of the magnetic flux created by a single conductor at a point $P$ of coordinates $(x_0, y_0, z_0)$. Figure 2 shows a graphical representation of the conductor and the coordinates system used for the analysis. According to previous work [33], the flux density

created by the conductor can be expressed as follows:

$$\vec{B} = \frac{\mu_0}{4\pi} \int_{-L}^{L} \frac{I \cdot d\vec{l} \wedge (\vec{r} - \vec{r}')}{|\vec{r} - \vec{r}'|^3} \tag{1}$$

$\vec{r}$ being the position vector of the differential element $d\vec{l}$ and $\vec{r}'$ the position vector of the $P$ point. According to Figure 2 the position vectors can be calculated as: $\vec{r} = l \cdot \vec{i} + a \cdot \vec{j}$ and $\vec{r}' = x_0 \cdot \vec{i} + y_0 \cdot \vec{j} + z_0 \cdot \vec{k}$. Therefore, the normal component of the flux density $B_y$ can be obtained by means of the following equation:

$$B_Y = \frac{\mu_0}{4\pi} \int_{-L}^{L} \frac{-z_0 \cdot I \cdot dl}{\left(\sqrt{(x_0 - l)^2 + (y_0 - a)^2 + z_0^2}\right)^3} \tag{2}$$

By integrating the above equation the flux density can be calculated as follows:

$$B_Y = \frac{\mu_0 \cdot I \cdot z_0}{4\pi \left((y_0 - a)^2 + z_0^2\right)} \left[\frac{x_0 - L}{\sqrt{(x_0 - L)^2 + (y_0 - a)^2 + z_0^2}} - \frac{x_0 + L}{\sqrt{(x_0 - L)^2 + (y_0 - a)^2 + z_0^2}}\right] \tag{3}$$

The above expression is simplified if the length of the conductor is not taken into account. In fact, if the conductor is considered to be infinite, the limit when $L \to \infty$ of Equation (3) must be calculated in order to obtain the flux density $B_y$. In this case, the result for the magnetic induction is the following:

$$B_Y = -\frac{\mu_0 \cdot I \cdot z_0}{2\pi \left((y_0 - a)^2 + z_0^2\right)} \tag{4}$$

Once the flux density created by a single infinite conductor has been obtained the following stage of the analysis process will consist of the calculation of the flux density created by a single layer of conductors. Figure 3(a) shows a diagram with the coordinates system and the layer of conductors. The total current of the layer, sum of the individual currents of each conductor, is designed by $I_T$.

The flux density created by the layer of conductors can be calculated by integrating Equation (4) along the $z$ axis (between 0 and $H$). To do this, a current differential element can be defined as the quotient between the total current and the height of the layer:

$$dI = \frac{I_T}{H} \cdot dz \tag{5}$$

The contribution of this differential current to the flux density $B_y$ at the point $P$ of coordinates $(x_0, y_0, z_0)$ can be easily calculated by means of Equation (4):

$$dB_Y = -\frac{\mu_0 \cdot I_{TOT} \cdot (z_0 - z) \cdot dz}{2\pi \cdot H \left((y_0 - a)^2 + z_0^2\right)} \tag{6}$$

Figure 3(b) shows the current differential element and the domain integration for the layer along the $z$ axis.

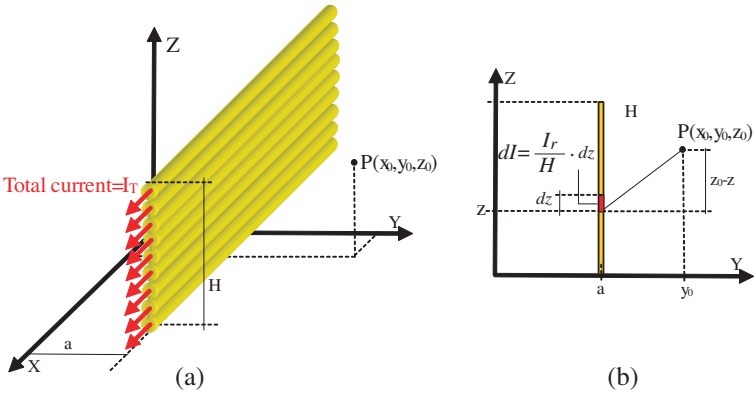


**Figure 3.** (a) Single layer of conductors and coordinates system. (b) Current differential element $dI$.

The total flux density $B_y$ of the layer can be then calculated as the following integral:

$$B_Y = -\frac{\mu_0 \cdot I_{TOT}}{2\pi \cdot H} \int_0^H \frac{(z_0 - z) \cdot dz}{\left((y_0 - a)^2 + z_0^2\right)} \tag{7}$$

Thus $B_y$ reaches the following value:

$$B_Y = -\frac{\mu_0 \cdot I_{TOT}}{2\pi \cdot H} \cdot \ln\left[\frac{(z_0 - H)^2 + (y_0 - a)^2}{(y_0 - a)^2 + z_0^2}\right] \tag{8}$$

The last stage to obtain an expression for the leakage flux produced by the simplified domain of Figure 1 will consists of the calculation of the flux density produced by multiple adjacent layers of conductors. Figure 4(a) shows a diagram with the layers distribution and Figure 4(b) shows the differential current element used to integrate the contribution of every layer along the $y$ axis.

The current differential element can be calculated by simply dividing the total current of all the layers between the width along

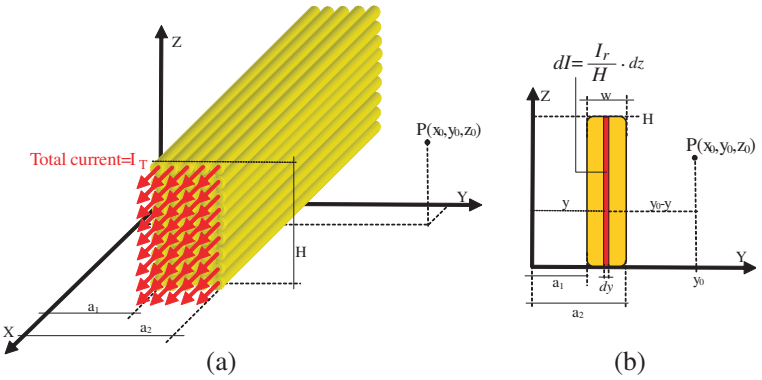


**Figure 4.** (a) Multiple layers of conductors and coordinate system. (b) Current differential element $dI$.

the $y$ axis ($w$) of the system of conductors:

$$dI = \frac{I_T}{w} \cdot dy \tag{9}$$

In this way, the contribution of this differential current to the flux density $B_y$ at the point $P$ can be easily calculated by means of Equation (8):

$$dB_Y = -\frac{\mu_0 \cdot I_{TOT}}{2\pi \cdot A \cdot H} \cdot dy \cdot \ln\left[\frac{(z_0 - H)^2 + (y_0 - y)^2}{(y_0 - y)^2 + z_0^2}\right] \tag{10}$$

Therefore, the total flux density created by multiple layers of conductors will be the following:

$$B_Y = -\frac{\mu_0 \cdot I_{TOT}}{2\pi \cdot A \cdot H} \cdot \int_{a_1}^{a_2} \ln\left[\frac{(z_0 - H)^2 + (y_0 - y)^2}{(y_0 - y)^2 + z_0^2}\right] \cdot dy \tag{11}$$

The integral of the above equation is simplified if the position of the coordinates system is slightly changed. For the particular case of $a_1 = 0$, $a_2 = W$ and $y_0 = W$ the set of conductors is located at the $X$ axis and the flux density $B_Y$ is calculated just in the external surface of the right layer of conductors. Under these conditions $B_Y$ can be calculated as:

$$B_Y = -\frac{\mu_0 \cdot I_{TOT}}{2 \cdot A \cdot H} \cdot \left[-W \cdot Ln\left|\frac{W^2 + z^2}{W^2 + (z - H)^2}\right| + \sum_{i=0,H} 2 \cdot (z - i) \cdot atg\left(\frac{W}{z - i}\right)\right] \tag{12}$$

This is the equation that allows the calculation of the flux density created by the simplified domain of Figure 1. In fact, only the dimensions $W$ and $H$ of the set of conductors are needed to obtain $B_Y$. Therefore, if $B_Y$ is calculated along the total height $H$ of the layers of conductors its symmetry can be established and thus the symmetry of the leakage flux created by the winding of a transformer will be also demonstrated. The simplest way to study the symmetry of $B_Y$ is plotting the function for a wide range of values of the variable $Z$:

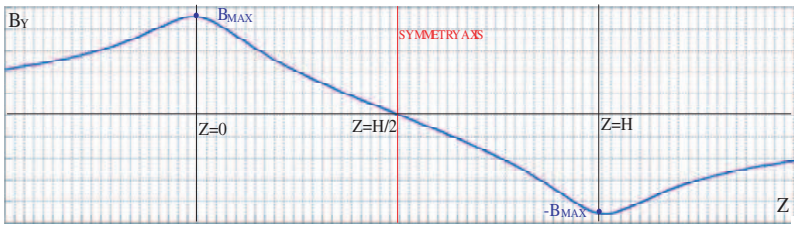


**Figure 5.** Flux density $B_y$ along a line parallel to the multiple layers of conductors ($Z$ axis).

In this plot, the axis of symmetry is clearly located at the middle of the height ($H/2$) of the set of conductors. The maximum flux density is reached at the two ends of the set of conductors. From these two points the magnetic flux slowly decreases to zero with the distance. These results can be directly extrapolated to the simplified domain of Figure 1 where two layers of conductors substitute the winding of the transformer. If this is done the symmetry of the leakage flux is also demonstrated. In fact, Figure 6 shows the flux density obtained for the transformer by means of Equation (12) applied to the simplified domain of Figure 1. The symmetry of leakage flux is clearly appreciated in Figure 6.

Once the spatial distribution of leakage flux density has been analytically calculated and its symmetrical nature has been demonstrated the foundations of a diagnosis method for the early detection of inter-turn insulation faults can be established. Leakage flux can be analysed by measuring the voltage it induces in very simple air core coils located at the surface of transformer windings. Figure 7 shows a diagram where the location of the coils and its equivalent circuit are presented. If coils are identical and symmetrically installed leakage flux will induce the same electromotive force in both coils. This fact is easily demonstrated since leakage flux is symmetrical for the surfaces covered by both coils.

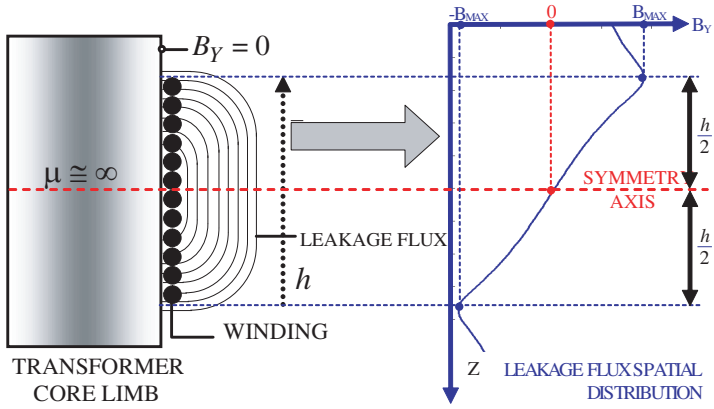


**Figure 6.** Symmetry of the leakage flux produced by a transformer core limb.

The diagnosis method will be thus based on the detection of changes caused in leakage flux line paths by the presence of the insulation failure. When a short-circuit, or even a strong deformation, of one or several turns occurs, the symmetry of the leakage flux is lost and the fault can be detected by measuring voltage changes induced in the sensors. In fact, the difference of the electromotive forces induced in the coils $V_{OUT}$ will be theoretically nil for a healthy transformer while it will present a value, proportional to the fault level, in the case of a faulty transformer. In practice, a healthy machine will produce a residual value of $V_{OUT}$ since neither the windings nor the coils can be built absolutely symmetrical. This offset value is not a problem for a correct diagnosis since it can be measured when the machine is installed and all the successive measures may be referred to it. In the following section finite elements simulations of real transformers with concentric and disc-type windings will be presented in order to analyse in depth the proposed method.

## 3. FAULT DIAGNOSIS ON LOW VOLTAGE MACHINES: SIMULATION AND EXPERIMENTAL RESULTS

Power transformers generally present two different structures in their windings: concentric layer windings and disc-type windings. Figure 8 shows these two types of winding. The concentric layer windings are built by winding several layers of conductor along the total length of the core limb. Primary and secondary windings are thus concentric and separated by an insulating material. Disc-type windings are formed by a set of discs. Every disc is toroidally wound around the core

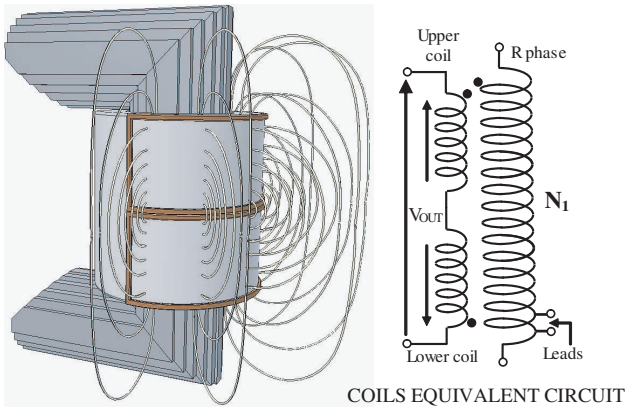


**Figure 7.** Air-core coils for the measurement of the leakage flux.

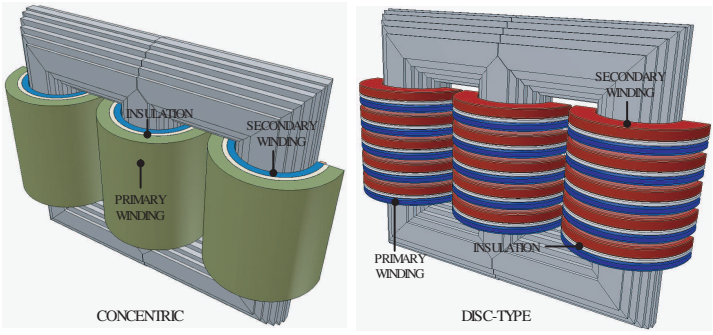


**Figure 8.** Concentric and disc-type windings.

and insulated from the others discs by means of a layer of insulating material. Primary and secondary windings are formed by the series connection of several discs that are usually alternatively distributed along the magnetic core limbs.

Simulation and experimental analysis have been carried out in both type of transformer in order to check the symmetry of the leakage flux as well as the reliability of the proposed method. For the experimental analysis two transformers of 12 kVA were built. Both machines incorporated a set of leads connected to the windings in order to apply inter-turn insulation faults. Figure 9 and Figure 10 show the external appearance of the transformers and their main specifications. In both cases the leads and connectors to apply inter-turn short-circuits are clearly visible.

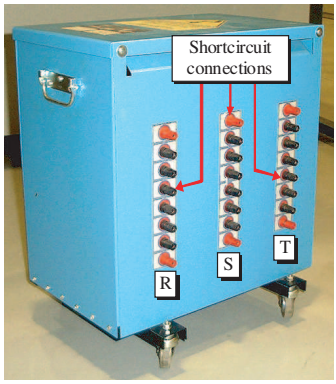


| | |
|---|---|
| Voltage | 400/400 Yy – 400/230 Yd |
| Apparent power | 12 kVA |
| Winding Conductors | 3.2 mm copper wire class H insulation |
| Primary winding turns | 183 Turns (3 Layers) |
| Secondary winding turns | 183 Turns (3 Layers) |
| Leads for short-circuit | Turns 1, 3, 7, 15, 31, 61 |
| Connection | Yy6 (Yy–Yd–Dy –Dd possible) |
| Magnetic Core | Cold laminated steel 0.86W/kg-0.33 mm |
| Winding insulation | Tercott CF™ (Polyester paper) |
| Core dimensions | 350 x 350 mm |
| Window dimensions | 210 mm |
| Magnetic flux density | 1.2 T (average) |
| Voltage per turn | 1.26 V |

**Figure 9.** Concentric windings experimental transformer.

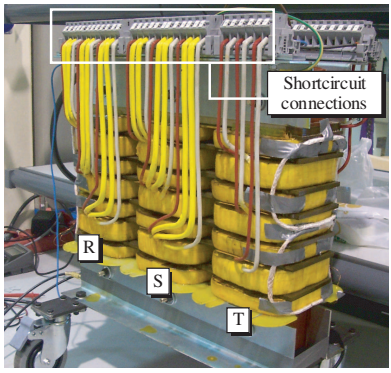


| | |
|---|---|
| Voltage | 400/400 Yy – 400/230 Yd |
| Apparent power | 12 kVA |
| Winding Conductors | 3 mm copper wire class H insulation |
| Primary winding discs | 4 Discs – Total turns=173. 7 Layers |
| Secondary winding discs | 3 Discs – Total turns=171. 6 Layers |
| Leads for short-circuit | Turns 1, 3, 7, 15, 31, 61 |
| Connection | Yy6 (Yy–Yd–Dy –Dd possible) |
| Magnetic Core | Cold laminated steel 0.86W/kg-0.33 mm |
| Winding insulation | Tercott CF™ (Polyester paper) |
| Core dimensions | 350 x 350 mm |
| Window dimensions | 80 mm |
| Magnetic flux density | 1.2 T (average) |
| Voltage per turn | 2.3 V aprox. |

**Figure 10.** Disc-type windings experimental transformer.

Although analytical methods are valid to solve complex electromagnetic problems [34–38] and some authors have even proposed new approaches [39], finite element method (FEM) has been proved as a very accurate technique for diagnosis and analysis of electromagnetic devices [41–44], especially in the field of electrical machines since it can include actual characteristics of the healthy and faulty machine [45–47]. Therefore, the theoretical study of leakage flux used for the development of the method was carried out by means of commercial software of electromagnetic analysis by the FEM. By means of the simulation of both transformers the symmetry of the leakage flux was checked as well as the capacity of the method to detect faults affecting a single turn with the transformer operating at different load levels [48]. In all the cases the simulation and experimental results

demonstrated it was possible to detect an insulation fault affecting only a single turn, even when the failure current was so strongly limited that the machine did not suffer any permanent damage. The successful detection under so adverse conditions ensures the capability of the method to detect the most incipient insulation faults in any industrial transformer.

In first place, the results of the finite element models will be presented in order to show the line paths of leakage flux in transformers with the most common types of winding. A perfect symmetry of leakage flux will be observed in all the cases prior to producing the insulation fault. However, once an insulation fault has occurred the leakage flux strongly increases in the region of the failure loosing this way its natural symmetry. Figures 11 and 12 present the results of the simulation of the concentric windings transformer and the disc-type windings transformer respectively. In these figures the leakage flux density (Wb/m) along a line parallel to the windings has been calculated in different time instances of the electrical cycle, for both the transformer operating in normal conditions and after producing an inter-turn short-circuit. The presented results clearly show the behaviour of the diagnosis method. In all the cases the flux density is symmetrical along the windings when the machines are healthy. However, if a single turn is short-circuited a strong concentration of flux appears in the region of the failure and leakage flux is no longer symmetrical. This change in the line paths of the leakage flux can be easily detected by means of the measurement of the induced electromotive force in coils installed at the winding surface (Figure 7). Therefore, it can be affirmed that simulation results clearly demonstrate the symmetry of the leakage flux for any type of winding

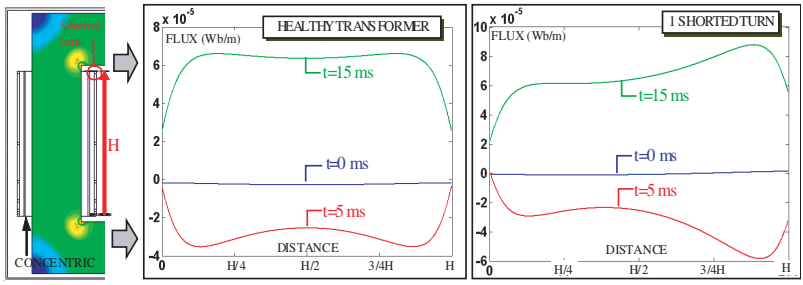


**Figure 11.** Leakage flux density along a line parallel to the winding of the R-phase of a concentric winding transformer in three different time instances of the electrical cycle.

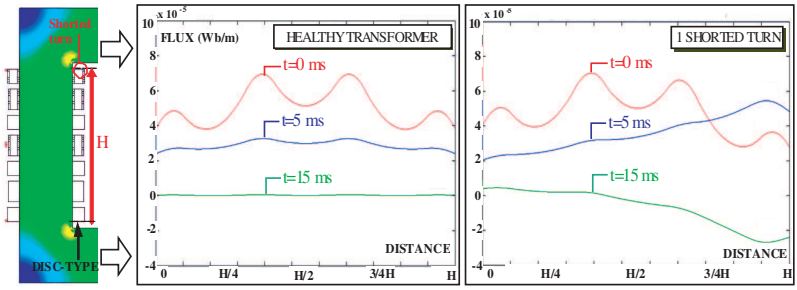


**Figure 12.** Leakage flux density along a line parallel to the winding of the R-phase of a disc-type winding transformer in three different time instances of the electrical cycle.

as well as the sensitivity of this variable to the presence of inter-turn short-circuits. Once the simulation has validated the theory about the leakage flux, experimental results will be presented.

Experimental tests were carried out on both transformers after installing a pair of coils in every phase. Coils were machine wound with 100 turns of insulated copper wire. All the tests were carried out with the failure current limited to 1.2 times the rated current of the windings. In this way, the machine integrity was completely preserved. Different load levels, from no load to the rated load, were applied to the tested transformers and the results demonstrated the influence of load in the diagnosis could be neglected. In all the cases the variable used to diagnose the insulation fault was the induced electromotive force $V_{OUT,}$ obtained as the sum of the electromotive forces induced in every single coil. This variable is close to zero when the windings are healthy and presents a significant value when an insulation fault exists. Figure 13 shows some of the results obtained for the concentric windings transformer before and after producing an inter-turn short-circuit in the R-phase with the machine operating at no load. The graphs show how the amplitude of the total electromotive force $V_{OUT}$ is almost 7 times higher when the fault is present, although the fault current has been limited to 1.2 the rated current of the windings. As explained in Section 1, the residual value of $V_{OUT}$ obtained for the healthy transformer (whose peak amplitude is only 22 mV), is caused by the asymmetries of both the transformer windings and the coils for leakage flux measurement.

Figure 14 shows the results obtained for the disc-type windings transformer. In this case, the fault indicator $V_{OUT}$ has been measured for the R and S-phases simultaneously, although the inter-turn insulation fault has been applied in the R-phase only. The results

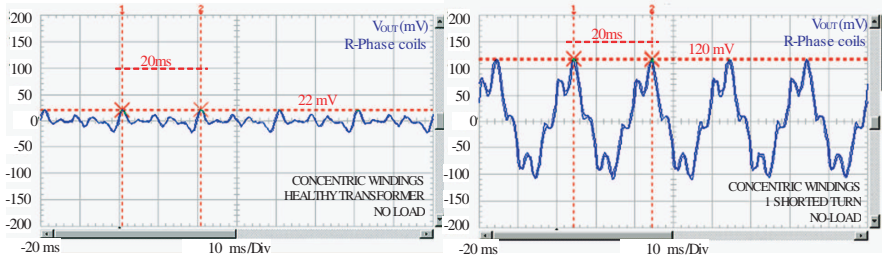


**Figure 13.** Experimental results: VOUT obtained for the concentric windings transformer before and after producing an inter-turn short-circuit affecting a single turn in the R-phase (transformer unloaded).

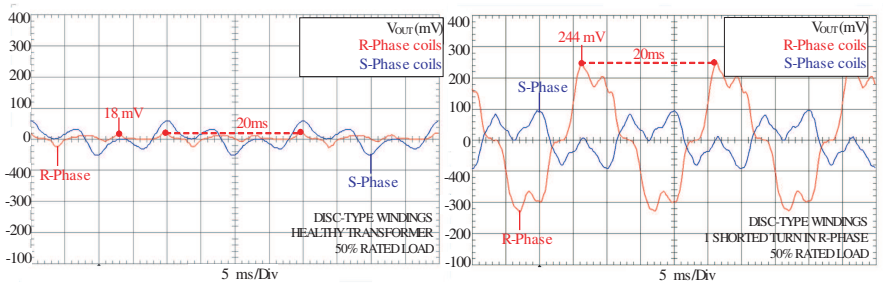


**Figure 14.** Experimental results: VOUT obtained for the disc-type windings transformer before and after producing an inter-turn short-circuit affecting a single turn in the R-phase (transformer operating at 50% of the rated load).

show, as in the previous case, a huge increase in the total electromotive force $V_{OUT}$ of the R-phase although the failure current has been also limited to 1.2 times the rated current. A very slight increase in the $V_{OUT}$ of the S-phase can also be detected. This minimum variation is caused by the influence of the leakage flux created by the fault of the R-phase on the measurement coils of the S-phase. This phenomenon has been observed in adjacent phases during the experimental tests but it does not create any drawback for the application of the method. The influence of one phase on the other is negligible if it is compared to the strong effect caused by the fault on the measurement coils of faulty phase. Moreover, the magnitude of the faults applied to the transformer is so low and the sensitivity of the method so high that no possibility of misinterpretation of the results exist.

## 4. FAULT DIAGNOSIS IN HIGH VOLTAGE MACHINES

In order to demonstrate the possibility of industrial application of the diagnosis method on large HV transformers, experimental tests were carried out on a large machine specially modified to apply inter-turn insulation faults. The transformer used for these tests was a 400 kVA–22 kV/400 V industrial transformer. Figure 15 shows the external aspect of the machine as well as its main technical specifications. The windings of this transformer were redesigned in order to install a series of leads, externally connected to a set of bushings, from which it is possible to short-circuit 1, or 2 turns in any phase of the machine. Figure 16 shows photographs of the original windings of the transformer and the new windings after installing the leads. Since the transformer is a high voltage machine and electrical insulation must be kept, the leads were connected to a set of new bushings installed in the top of the machine casing. In this way, by simply connecting a resistance between the new bushings it was possible to limit the failure current of the inter-turn short-circuit to the desired value. The new bushings can be observed in the photograph of Figure 15. In order to measure the leakage flux two coils manufactured with 100 turns of copper wire were also installed at the surface of the windings.


| | |
|---|---|
| Voltage | 2200/400 Dy |
| Apparent power | 400 kVA |
| Winding Conductors | 1.4 mm copper wire class H insulation |
| Intensity | 10,5 A / 577 A |
| Tap changer | 2.5% - 5% |
| Primary winding turns | 2300 Turns (11 Layers) |
| Secondary winding turns | 23 Turns (23 Layers) |
| Leads for short-circuit | Turns 1, 3 |
| Winding insulation | Paper – (oil immersed) |
| Core dimensions | 870 x 752 mm |
| Window dimensions | 372 mm |
| Magnetic flux density | 1.2 T (average) |
| Voltage per turn primary | 0.96 V |

**Figure 15.** High voltage transformer used for the experimental tests.

Since the coils were installed at the surface of the windings they were insulated by means of high voltage mica-epoxy tape. In this way, the induced electromotive force measured by them was easily transferred to the outside of the machine. Figure 17 shows two photographs of the installation of the flux measurement coils. In


**Figure 16.** Modification of the windings for the installation of the short-circuit leads.

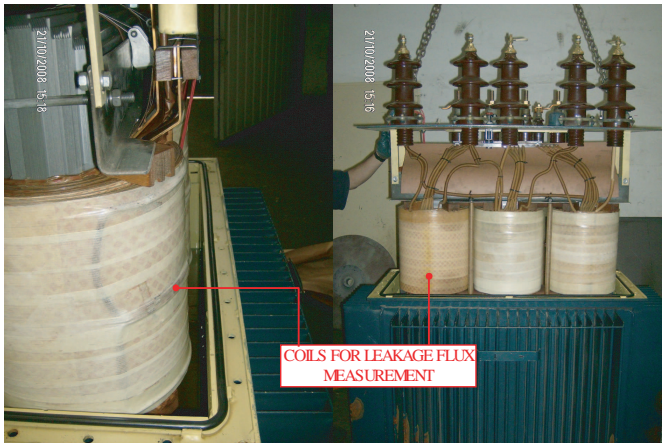


**Figure 17.** Installation of the flux measurement coils.

the left-side photograph the coils of the R-phase of the machine can be observed under the mica-epoxy tape used as insulation. Figure 18 shows a diagram where the location of coils for leakage flux measurement and the internal structure of the windings of the monitored transformer are clearly presented.

Once the machine used in the experimental tests has been fully described the results obtained in the diagnosis of insulation faults will be presented. It is important to point out that because of the high power (400 kVA) of the machine the experimental tests could only be done with the machine unloaded. This restriction is not a drawback for the implementation of the method in large HV transformers since previous tests and simulations carried out in low voltages machines demonstrated the effect of load on the proposed diagnosis method is negligible. In fact, although Figures 13 and 14 show results obtained

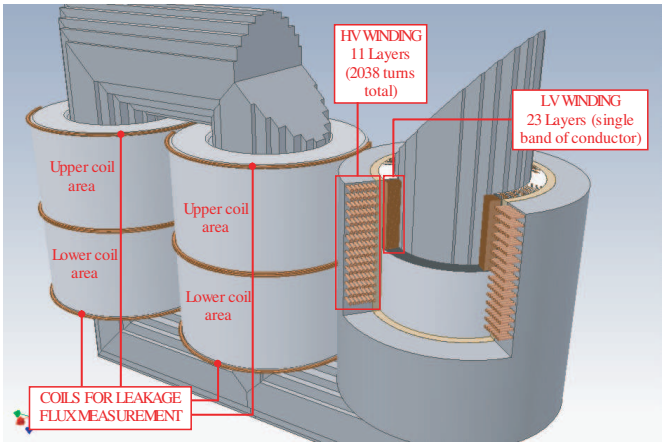


**Figure 18.** Structure of the windings and location of the flux measurement coils.

with no load and with the 50% of the rated load respectively the evolution of the output variable $V_{OUT}$ can be considered identical in both cases.

Taking into account that the aim of the new diagnosis method is the early detection of incipient faults, all the tests were performed with only a shorted turn. Moreover, the short-circuit current flowing through the faulty turn was limited to 2 times the rated current. In fact, fault current was limited to 21 A for a turn of the primary winding that in rated conditions must carry 10.5 A. Therefore, if this low level of fault is detected the sensitivity of the method will be clearly demonstrated as well as its capacity for the diagnosis of very incipient insulation faults.

Figure 19 shows the results obtained during the test. In this graph the sum of the electromotive forces induced in the pair of coils installed at the R-phase ($V_{OUT}$) is presented before and after applying the insulation fault. The graph clearly shows an important increase in this variable when the insulation fault is present.

If the $V_{OUT}$ signal is processed, a DC voltage level can be obtained as a severity factor that is much clearer than the visual evaluation of the waveforms. The processing required is extremely simple, as only rectification and low pass filtering of the voltage signals are needed to obtain a DC voltage related to the failure level of the machine. This processing of the signal can be easily done by hardware or software. If a software processing is applied the severity factor $\Delta$ can be obtained

according to Equation (13):

$$\Delta = \frac{1}{T}\int_{0}^{T} |V_{OUT}(t)| \cdot dt \tag{13}$$

Which indicates $\Delta$ can be calculated as the mean value of the absolute value of the signal $V_{OUT}$. Obviously, the effect of this operation on the signal is identical to the rectifying and filtering described above: the absolute value of $V_{OUT}$ is identical to the rectified signal and the calculation of its mean value is equivalent to the application of a low-pass filter.

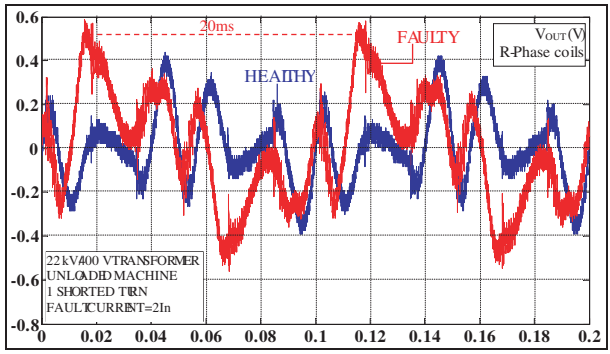


**Figure 19.** Results obtained for the HV transformer with a single shorted turn and the failure current limited to 2 times the rated current.

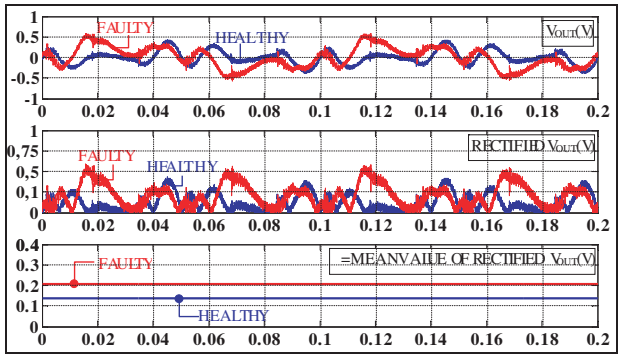


**Figure 20.** Calculation of the severity factor. Results obtained for the HV transformer with a single shorted turn and the failure current limited to 2 times the rated current.

Figure 20 graphically shows the procedure for the calculation of the severity factor. In first place the $V_{OUT}$ signals obtained for the healthy and faulty machine are represented. Both signals are then rectified and the mean value of the rectified signals is finally calculated. The graph clearly shows how the severity factor almost increases a 100% when the insulation fault exists. Therefore, the obtained results confirm the ability to detect minor insulation faults by simply evaluating this DC indicator. Moreover, the calculation of $\Delta$ is extremely easy by means of conventional integrated circuits. In this way, the installation of a monitoring device in any transformer is straightforward.

## 5. CONCLUSIONS

By means of the theory of the electromagnetic images an approximate analytical analysis of the leakage flux created by the windings of a power transformer has been carried out. This study shows that leakage flux distribution in three-phase transformers has a horizontal symmetry axis which passes through the middle-height of the magnetic core. FEM models of power transformers with different type of windings have been also designed and checked by comparing its results with real laboratory measurements. By means of these models, a complete study of the path defined by leakage flux lines of the transformer operating at different time instants has been carried out. The results of this study demonstrate this symmetrical distribution is maintained at all times during the supply cycle of the machine independently of the type of winding. It has also been demonstrated that leakage flux symmetry is automatically lost when an inter-turn short-circuit exists in the transformer windings. Therefore, leakage flux can be easily applied for the early detection of this type of failure.

Both simulation and experimental results show that the use of two air core coils magnetically coupled to the transformer windings allows direct, reliable and precise detection of leakage flux changes. It has also been demonstrated that the combined use of two coils attached to the windings surface permits the detection of a single shorted turn, even when the failure current is limited to values that are almost identical to the rated ones for the faulty turn.

The diagnosis procedure has been successfully applied to a large HV power transformer in which a very incipient insulation fault has been easily detected. It has also been demonstrated that very simple signal processing techniques applied to the voltage induced in coils allow the calculation of a DC voltage value that is much higher in the faulty machine than in normal operation. Therefore, an excellent,

sensitive severity factor for this failure can be easily obtained and the method easily extended to any industrial machine.

## ACKNOWLEDGMENT

The authors gratefully acknowledge the financial support of the Spanish National Plan of Research and Development and the company TSK Electrónica y Electricidad for the development of the present study.

## REFERENCES

1. Faghihi, F. and H. Heydari, "Reduction of leakage magnetic field in electromagnetic systems based on active shielding concept verified by eigenvalue analysis," *Progress In Electromagnetics Research*, Vol. 96, 217–236, 2009.
2. Fang, C.-H., S. Zheng, H. Tan, D. Xie, and Q. Zhang, "Shielding effectiveness measurements on enclosures with various apertures by both mode-tuned reverberation chamber and gtem cell methodologies," *Progress In Electromagnetics Research B*, Vol. 2, 103–114, 2008.
3. Bahadorzadeh Ghandehari, M., M. Naser-Moghadasi, and A. R. Attari, "Improving of shielding effectiveness of a rectangular metallic enclosure with aperture by using extra wall," *Progress In Electromagnetics Research Letters*, Vol. 1, 45–50, 2008.
4. Lei, J.-Z., C. H. Liang, and Y. Zhang, "Study on shielding effectiveness of metallic cavities with apertures by combining parallel FDTD method with windowing technique," *Progress In Electromagnetics Research*, Vol. 74, 85–112, 2007.
5. Atherton, D. L., "Magnetic inspection is key to ensuring safe pipelines," *Oil & Gas Journal*, Vol. 87, No. 32, 52–61, August 1989.
6. Yamada, S., M. Katou, M. Iwahara, and F. P. Dawson, "Eddy current testing probe composed of planar coils," *IEEE Transactions on Magnetics*, Vol. 31, No. 6, Part 1, 3185–3187, November 1995.
7. Mandal, K., D. Dufour, and D. L. Atherton, "Use of magnetic Barkhausen noise and magnetic flux leakage signals for analysis of defects in pipeline steel," *IEEE Transactions on Magnetics*, Vol. 35, No. 3, Part 2, 2007–2017, May 1999.
8. Yamada, S., H. Fujiki, M. Iwahara, S. C. Mukhopadhyay, and F. P. Dawson, "Investigation of printed wiring board testing

by using planar coil type ECT probe," *IEEE Transactions on Magnetics*, Vol. 33, No. 5, Part 1, 3376–3378, September 1997.

9. Dogaru, T. and S. T. Smith, "Giant magnetoresistance-based eddy-current sensor," *IEEE Transactions on Magnetics*, Vol. 37, No. 5, Part 2, 3831–3838, September 2001.
10. Yamada, S., K. Chomsuwan, Y. Fukuda, M. Iwahara, H. Wakiwaka, and S. Shoji, "Eddy-current testing probe with spin-valve type GMR sensor for printed circuit board inspection," *IEEE Transactions on Magnetics*, Vol. 40, No. 4, Part 2, 2676–2678, July 2004.
11. Chomsuwan, K., S. Yamada, M. Iwahara, H. Wakiwaka, and S. Shoji, "Application of eddy-current testing technique for high-density double-layer printed circuit board inspection," *IEEE Transactions on Magnetics*, Vol. 41, No. 10, 3619–3621, October 2005.
12. Jordan, H. and F. Taegen, "Wellenflusse infolge von Schwankungen des Luftspaltenwertes," *Elektrotech. Z*, Vol. 85, 865–867, 1964.
13. Erlicki, M. S., Y. Porat, and A. Alexandrovitz, "Leakage field changes of an induction motor as indication of nonsymmetric supply," *IEEE Trans. Ind. Gen. Appl.*, Vol. 7, No. 6, 713–717, November/December 1971.
14. Cabanas, M. F., M. G. Melero, G. A. Orcajo, F. Rodríguez Faya, and J. Solares, "Experimental application of the axial leakage flux to the detection of rotor asymmetries, mechanical anomalies and interturn shortcircuits in working induction motors," *Proc. of International Conference on Electrical Machines, ICEM'98*, 420–425, Istanbul, 1998.
15. Penman, J., H. Sedding, B. Lloyd, and W. Fink, "Detection and location of interturn shortcircuits in the stator winding of operating motors," *IEEE Trans. on Energy Conversión*, Vol. 9, No. 4, December 1994.
16. Vas, P., *Parameter Estimation, Condition Monitoring and Diagnosis of Electrical Machines*, Oxford University Press, 1993, ISBN 0-19-859375-9.
17. ANSI/IEEE, "IEEE guide for the interpretation of gases generated in oil-inmersed transformers," IEEE Power Engineering Society, 1992.
18. IEC Publication 599, *Interpretation of the Analysis of Gases in Transformers and Other Oil-filled Electrical Equipment in Service*, 1st Edition, 1978.
19. Rogers, R. R., "IEEE and IEC Codes to interpret incipient faults

in transformers using gas in oil analyis," *IEEE Transactions on Electrical Insulation*, Vol. 13, No. 5, 1978.

20. Yang, H.-T. and C.-C. Liao, "Adaptive fuzzy diagnosis system for dissolved gas analysis of power transformers," *IEEE Transactions on Power Delivery*, Vol. 14, No. 4, October 1999.
21. Kreuger, F. H., *Partial Discharge Detection in High-voltage Equipment*, Ed. Butterworths, 1989, ISBN 0-408-02063-6.
22. Aschenbrenner, D., H. G. Kranz, W. R. Rutgers, and P. Van den Aardweg, "On-line PD measurements and diagnosis on power transformers," *IEEE Transactions on Dielectrics and Electrical Insulation*, Vol. 12, No. 2, 216–221, April 2005.
23. Turley, M. F., "Los ensayos de tangente de delta en campo como herramienta para la evaluación del estado del aislamiento de equipos eléctricos de alta tensión," *International Conference of Electrical Insulation (Jornadas Internacionales sobre aislamiento Eléctrico) Labein*, IEEE Power Engineering Society, Spanish Chapter, Bilbao, September 1994.
24. Ward, B. H., "A survey of new techniques in insulation monitoring of power transformers," *IEEE Electrical Insulation Magazine*, Vol. 17, No. 3, 16–23, May/June 2001.
25. Saha, T. K., "Review of modern diagnostic techniques for assessing insulation condition in aged transformers," *IEEE Transactions on Dielectrics and Electrical Insulation*, Vol. 10, No. 5, 903–916, October 2003.
26. Van Bolhuis, J. P., E. Gushki, and J. J. Smith, "Monitoring and diagnostic of transformer solid insulation," *IEEE Transactions on Power Deliver*, Vol. 17, No. 2, 528–536, April 2002.
27. Chapman, S. J., *Electric Machinery Fundamentals*, International Edition, Mc Graw Hill, 2003, ISBN 0-07-Y66160.
28. Reitz, J. R. and F. J. Milford, *Foundations of Electromagnetic Theory*, UTEHA, 2008, ISBN 84-274-0702.
29. Dormont, M. J., "Cálculo y Construcción de las Máquinas Eléctricas Estáticas," Universidad Politécnica de Madrid — Escuela Técnica Superior de Ingenieros Industriales, Sección de publicaciones.
30. Kong, J. A., *Electromagnetic Wave Theory*, 2nd edition, 364–371, Wiley, New York, 1990.
31. De Leon, F. and A. Semlyen, "Efficient calculation of elementary parameters of transformers," *Transactions on Power Delivery*, Vol. 7, No. 1, January 1992.
32. Kladas, A. G., M. P. Papadopoulos, and J. A. Tegopoulos,

"Leakage flux and force calculation on power transformer windings under short-circuit: 2D and 3D models based on the theory of images and the finite element method compared to measurements," *IEEE Transactions on Magnetics*, Vol. 30, No. 5, September 1994.

33. Rodriguez, V. L., "Electromagnetismo," Universidad Nacional de Educación a Distancia (UNED), 2002, ISBN: 84-362-4680-2.
34. Lecointe, J.-P., B. Cassoret, and J. F. Brudny, "Distinction of toothing and saturation effects on magnetic noise of induction motors," *Progress In Electromagnetics Research*, Vol. 112, 125–137, 2011.
35. Ravaud, R. and G. Lemarquand, "Magnetic field produced by a parallelepipedic magnet of various and uniform polarization," *Progress In Electromagnetics Research*, Vol. 98, 207–219, 2009.
36. Ravaud, R. and G. Lemarquand, "Comparison of the coulombian and amperian current models for calculating the magnetic field produced by radially magnetized arc-shaped permanent magnets," *Progress In Electromagnetics Research*, Vol. 95, 309–327, 2009.
37. Akyel, C., S. I. Babic, and M.-M. Mahmoudi, "Mutual inductance calculation for noncoaxial circular air coils with parallel axes," *Progress In Electromagnetics Research*, Vol. 91, 287–301, 2009.
38. Jian, L. and K.-T. Chau, "Analytical calculation of magnetic field distribution in coaxial magnetic gears," *Progress In Electromagnetics Research*, Vol. 92, 1–16, 2009.
39. Chen, J. and Q. H. Liu, "A non-spurious vector spectral element method for Maxwell's equations," *Progress In Electromagnetics Research*, Vol. 96, 205–215, 2009.
40. Touati, S., R. Ibtiouen, O. Touhami, and A. Djerdir, "Experimental investigation and optimization of permanent magnet motor based on coupling boundary element method with permeances network," *Progress In Electromagnetics Research*, Vol. 111, 71–90, 2011.
41. Torkaman, H. and E. Afjei, "FEM analysis of angular misalignment fault in SRM magnetostatic characteristics," *Progress In Electromagnetics Research*, Vol. 104, 31–48, 2010.
42. Torkaman, H. and E. Afjei, "Hybrid method of obtaining degrees of freedom for radial airgap length in SRM under normal and faulty conditions based on magnetiostatic model," *Progress In Electromagnetics Research*, Vol. 100, 37–54, 2010.
43. Torkaman, H. and E. Afjei, "Magnetio static field analysis regarding the effects of dynamic eccentricity in switched reluctance

motor," *Progress In Electromagnetics Research M*, Vol. 8, 163–180, 2009.

44. Afjei, E. and H. Torkaman, "The novel two phase field-assisted hybrid SRG: Magnetio static field analysis, simulation, and experimental confirmation," *Progress In Electromagnetics Research B*, Vol. 18, 25–42, 2009.
45. Faiz, J. and B. M. Ebrahimi, "Mixed fault diagnosis in three-phase squirrel-cage induction motor using analysis of air-gap magnetic field," *Progress In Electromagnetics Research*, Vol. 64, 239–255, 2006.
46. Faiz, J., B. M. Ebrahimi, and M. B. B. Sharifian, "Time stepping finite element analysis of broken bars fault in a three-phase squirrel-cage induction motor," *Progress In Electromagnetics Research*, Vol. 68, 53–70, 2007.
47. Vaseghi, B., N. Takorabet, and F. Meibody-Tabar, "Transient finite element analysis of induction machines with stator winding turn fault," *Progress In Electromagnetics Research*, Vol. 95, 1–18, 2009.
48. Cabanas, M. F., M. G. Melero, F. Pedrayes, C. H. Rojas, G. A. Orcajo, J. M. Cano, and J. G. Iglesias, "A new online method based on leakage flux analysis for the early detection and location of insulating failures in power transformers: Application to remote condition monitoring," *IEEE Transactions on Power Delivery*, Vol. 22, No. 3, 2007.